Large negative velocity gradients in Burgers turbulence

A. I. Chernykh[1,2,*] and M. G. Stepanov[1,2,3,†]
[1]*Institute of Automation and Electrometry, Novosibirsk 630090, Russia*
[2]*Novosibirsk State University, Novosibirsk 630090, Russia*
[3]*Physics of Complex Systems, Weizmann Institute of Science, Rehovot 76100, Israel*
(Received 4 April 2000; revised manuscript received 23 February 2001; published 20 July 2001)

We consider one-dimensional Burgers equation driven by large-scale white-in-time random force. The tails of the velocity gradients probability distribution function (PDF) are analyzed by saddle point approximation in the path integral describing the velocity statistics. The structure of the saddle-point (instanton), that is, the velocity field configuration realizing the maximum of probability, is studied numerically in details. The numerical results allow us to find analytical solution for the long-time part of the instanton. Its careful analysis confirms the result of Balkovsky *et al.* [Phys. Rev. Lett. **78**, 1452 (1997)] based on short-time estimations that the left tail of PDF has the form $\ln \mathcal{P}(u_x) \propto -|u_x|^{3/2}$.

DOI: 10.1103/PhysRevE.64.026306 PACS number(s): 47.27.Gs, 05.10.−a

I. INTRODUCTION

We consider the random forced Burgers equation

$$u_t + uu_x - \nu u_{xx} = \phi \tag{1}$$

that describes weak one-dimensional (1D) acoustic perturbations in the reference frame moving with the sound velocity [1]. The external force ϕ in this frame is generally short correlated in time, so let us assume that

$$\langle \phi(x_1,t_1)\phi(x_2,t_2)\rangle = \delta(t_1-t_2)\chi(x_1-x_2). \tag{2}$$

Then the statistics of ϕ can be thought Gaussian and therefore is completely characterized by Eq. (2). We are interested in turbulence with a large value of Reynolds number $\mathrm{Re} = [\chi(0)L^4]^{1/3}/\nu$, where L is the characteristic scale of the stirring force correlator $\chi(x)$. This problem was intensively studied during the last years [2–7].

The main feature of Burgers turbulence is the formation of shock waves with large negative velocity gradient inside and small viscous width of the front. The positive velocity gradients are decreased by the dynamics of Burgers equation due to self-advection of velocity. On the contrary the increasing of negative gradients could be stopped only by viscosity. The motion of shock waves leads to a strong intermittency, the PDF of velocity gradients $\mathcal{P}(u_x)$ is strongly non-Gaussian. The one way to describe the intermittency is to study rare events with large fluctuations of velocity, that give the main contribution to the high momenta $\langle u_x^n \rangle$ or to the PDF tails.

The right tail (positive large u_x) of PDF $\ln \mathcal{P}(u_x) \propto -u_x^3$ was first found by Feigel'man [8] for the problem of charge density wave in an impurity potential. Later it was recovered using operator product expansion [2] (see also Ref. [5]), instanton calculus [3], minimizers approach [6], and mapping closure [7]. The left tail in the inviscid limit seems to be algebraic, probably $\mathcal{P}(u_x) \propto |u_x|^{-7/2}$ [6] (see also Refs. [7,9]). Due to viscosity the very far left tail is stretched exponential $\ln \mathcal{P}(u_x) \propto -\nu^3 |u_x/\nu|^\beta$. The large negative gradients exist practically only inside the shock waves. The maximal value of gradient is proportional to the square of the velocity jump on the shock wave $|u_x|_{\max} = (\Delta u)^2/8\nu$. Then roughly the tail of the shock wave amplitude PDF has the form $\ln \mathcal{P}_{\mathrm{shock}}(\Delta u) \propto -\nu^{3-2\beta}(\Delta u)^{2\beta}$. The analysis of the instanton structure predicts the value $\beta = 3/2$ [4]. This prediction is consistent with the assumption, that the tails of $\mathcal{P}_{\mathrm{shock}}(\Delta u)$ should not depend on the viscousity ν.

We are interested in the statistics of large values of gradients $u_x \gg u_{\mathrm{r.m.s.}}/L \sim [\chi(0)/L^2]^{1/3}$. The velocity field configurations $u(x,t)$ that make a contribution to the probability $\mathcal{P}(a)$ of the equality $u_x(0,0) = a$ have the gradient greater or equal to a somewhere. The probability $\mathcal{P}(a)$ decays very fast while a increases, i.e., the contribution of events with gradient greater than a somewhere is highly suppressed. Then one believes that only some specific field configurations $u(x,t,a)$ (''optimal fluctuations'' [10] or instantons) make contribution to $\mathcal{P}(a)$ at large $a > (u_{\mathrm{r.m.s.}}/L)\mathrm{Re}$. Under this assumption to calculate $\mathcal{P}(a)$ one should find this optimal field configuration $u(x,t,a)$ and estimate the probability of its realization.

All instantons of this type are posed at the far tail of the statistical weight of averaging $\mu[\phi(x,t)]$. Indeed, to produce large fluctuation of u the stirring force ϕ also should be large, and the probability of such fluctuation ϕ is low. The weight $\mu[\phi]$ may not contain a large parameter, but it should have fast tails, e.g., exponential ones. Then the concurrence between statistical weight and the value of calculated quantity makes the contributing realizations of $\phi(x,t)$ rather determined. This approach was introduced by Lifshitz [10]. Later it was applied to determine high order correlation functions in field theory [11] and in the systems of hydrodynamic type: simultaneous (see, e.g., Refs. [12,3,13]) and nonsimultaneous [14] ones.

The paper is organized as follows. In Sec. II we derive the equations for the instanton. Section III is devoted to the detailed description of our scheme of numerical calculations. In Sec. IV we discuss the numerical results and describe the behavior of the solution of instanton equations at large times.

*Email address: Chernykh@iae.nsk.su
†Email address: Stepanov@iae.nsk.su

II. SADDLE-POINT APPROXIMATION

The velocity gradients PDF $\mathcal{P}(a)$ can be written as the path integral

$$\mathcal{P}(a)=\langle\delta[u_x(0,0)-a]\rangle_\phi = \int \mathcal{D}u\mathcal{D}p\int_{-i\infty}^{i\infty} d\mathcal{F}\exp\{-\mathcal{S}+4\nu^2\mathcal{F}[u_x(0,0)-a]\}, \tag{3}$$

where the effective action $\mathcal{S}$ has the form [15,12]

$$\mathcal{S}=\tfrac{1}{2}\int_{-\infty}^{0}dt\int dx_1dx_2\,p(x_1,t)\chi(x_1-x_2)p(x_2,t) -i\int_{-\infty}^{0}dt\int dx\,p(u_t+uu_x-\nu u_{xx}). \tag{4}$$

The integration over $\mathcal{F}$ gives rise to $\delta[u_x(0,0)-a]$, and the factor $4\nu^2$ was chosen for our convenience. Note that if retarded regularization of the path integral (3) is used then $\int\mathcal{D}u\mathcal{D}p\exp(-\mathcal{S})=1$ and we have no normalizing u-dependent denominators in Eq. (3). One can find some analogies between the appearance of the second field p and technique that was developed by Keldysh [16] for nonequilibrium dynamics description.

We are interested in the tails of PDF $\mathcal{P}(a)$, i.e., the parameter a in the integral (3) is large. The asymptotics of $\mathcal{P}(a)$ at large $|a|\gg[\chi(0)L]^{2/3}/\nu$ is determined by the saddle-point configuration of fields $u(x,t)$, $p(x,t)$ (and also parameter $\mathcal{F}$), near which the variation of the integrand is equal to zero [12]. The saddle-point configuration (sometimes called classical trajectory or instanton) is governed by the following equations:

$$u_t+uu_x-\nu u_{xx}=-i\chi^*p, \tag{5}$$

$$p_t+up_x+\nu p_{xx}=4i\nu^2\mathcal{F}\delta(t)\delta'(x), \tag{6}$$

where χ^*p is the convolution

$$(\chi^*p)(x)=\int dx'\,\chi(x-x')p(x'). \tag{7}$$

The solution should satisfy boundary conditions

$$\lim_{t\to-\infty}u(x,t)=0,\quad \lim_{t\to+0}p(x,t)=0, \qquad \lim_{|x|\to\infty}u(x,t)=0,\quad \lim_{|x|\to\infty}p(x,t)=0. \tag{8}$$

The value of $\mathcal{F}$ is tuned in such a way that the condition $u_x(0,0)=a$ holds. The quantity $\mathcal{F}$ is a Lagrange multiplier for finding the extremum of $\mathcal{S}$ with the condition $u_x(0,0)=a$.

The equation for p should be solved moving back in time because of the signs at p_t and p_{xx} in the instanton equation (6). The convolution $-i\chi^*p$ is the optimal configuration of external force ϕ that produces large negative gradient.

In what follows we will measure the length in L units, i.e., we set $L=1$. Rescaling the time t and fields u, p one can exclude the parameter ν from the instanton equations

$$t=T/2\nu,\quad u=2\nu U,\quad p=4i\nu^2P,\quad a=2\nu A, \tag{9}$$

$$U_T+UU_x-\tfrac{1}{2}U_{xx}=\int dx'\,\chi(x-x')P(x'), \tag{10}$$

$$P_T+UP_x+\tfrac{1}{2}P_{xx}=\mathcal{F}\delta(T)\delta'(x), \tag{11}$$

at $T=0$ one has $U_x(0,0)=A$. The only parameter in the instanton equations is $A=a/2\nu$. Note that the steady-state kink solution of Burgers equation with the negative gradient a is

$$u=-\sqrt{2\nu|a|}\tanh(\sqrt{|a|/2\nu}x). \tag{12}$$

Thus the physical meaning of $|A|$ is the square of the ratio of pumping scale $L=1$ and the kink width $w_{\rm kink}=1/\sqrt{|A|}$.

The effective action $\mathcal{S}_{\rm extr}$ at the instanton that gives the right exponent

$$\ln\mathcal{P}(a)\simeq-\mathcal{S}_{\rm extr}(a) \tag{13}$$

is equal to

$$\mathcal{S}_{\rm extr}=-\tfrac{1}{2}\int_{-\infty}^{0}dt\int dx_1dx_2\,p(x_1,t)\chi(x_1-x_2)p(x_2,t) =4\nu^3\int_{-\infty}^{0}dT\int dx_1dx_2P(x_1,T)\chi(x_1-x_2)P(x_2,T). \tag{14}$$

The freedom of rescaling the fields u, p and the time t with appropriate change of ν gives us the following relation:

$$\mathcal{S}_{\rm extr}(a)=8\nu^3S(a/2\nu)=(2\nu)^3S(A), \tag{15}$$

with the function $S(A)$ to be determined. One can prove by straightforward calculation the following relation between functions $\mathcal{F}(A)$ and $S(A)$:

$$\mathcal{F}(A)=\frac{dS(A)}{dA}. \tag{16}$$

The relations of such sort are well known in classical mechanics; here A and $\mathcal{F}$ are conjugate variables, and saddle-point configuration is the trajectory of extremal action.

The instanton equations (10),(11) are Hamiltonian:

$$U_T(x,T)=-\frac{\delta\mathcal{H}}{\delta P(x,T)},\quad P_T(x,T)=\frac{\delta\mathcal{H}}{\delta U(x,T)}, \tag{17}$$

$$\mathcal{H}=\int dx\,P(UU_x-\tfrac{1}{2}U_{xx}-\tfrac{1}{2}\chi^*P). \tag{18}$$

The Hamiltonian $\mathcal{H}$ is the integral of motion, i.e., $d\mathcal{H}/dT=0$. Since both U and P tend to zero at $T\to-\infty$ we have $\mathcal{H}=0$. From the instanton equations and the condition $\mathcal{H}=0$ we get

$$S=\frac{\mathcal{F}A}{2}+\tfrac{1}{4}\int dTdx\, P_x U^2=\frac{\mathcal{F}A}{3}+\tfrac{1}{6}\int dTdx\, P_x U_x. \tag{19}$$

The last term is due to viscousity. At the right tail it is unimportant, and we have $dS/dA=3S/A$, i.e., $S\propto A^3$. At the viscous left tail its contribution to the action is of the same order as other terms. If $\ln\mathcal{P}(a)$ is a powerlike function: $\ln\mathcal{P}(a)\propto|a|^\beta$, then one has $\int dTdx\, P_x U_x=2(3-\beta)S$.

The high momenta can be calculated by the instanton method in a following way. Because $a^n\mathcal{P}(a)$ is a narrow function for large n, and only narrow velocity interval, which position depends on n, contributes to $\langle a^n\rangle$. The position of this interval is exactly the saddle point in the integral $\langle a^n\rangle \propto\int da\, a^n\exp[-\mathcal{S}_{\rm extr}(a)]$ [see Eq. (13)], that satisfies the equation

$$n=a\frac{d\mathcal{S}_{\rm extr}(a)}{da}=8\nu^3 A\frac{dS(A)}{dA}. \tag{20}$$

Combining it with $\mathcal{F}=n/8\nu^3A$ we again get Eq. (16). To get the instanton equations for the average $\langle a^n\rangle$ one should only substitute $\mathcal{F}$ in Eq. (11) for $n/8\nu^3A$. Then the instanton equations become the same as in Ref. [4].

One also should consider fluctuations near the instanton as a background. The way how the fluctuations can be taken into account is unknown yet but their influence to $\ln\mathcal{P}(a)$ due to their phase volume is small in comparison with $\mathcal{S}_{\rm extr}$ while $a\gg(u_{\rm rms}/L)$ Re. At smaller gradients the fluctuations essentially change the answer and we have the algebraic tail [6].

III. NUMERICAL CALCULATIONS

The preliminary calculations that were made in x, T variables have shown that the width of the instanton equations solution grows with $|T|$ and is proportional to $|T|^{1/2}$, while its amplitude is proportional to $|T|^{-1/2}$. To avoid the necessity of treating simultaneously narrow structure at small T and wide one at large T we used the following variables:

$$x=\xi\sqrt{T_0-T},\quad T=T_0(1-e^{-\tau}), \tag{21}$$

$$U=\tilde U/\sqrt{T_0-T},\quad P=\tilde P/\sqrt{T_0-T}, \tag{22}$$

where T_0 is some constant of the order of unity. The instanton equations in these variables take the form

$$\tilde U_\tau+\tfrac{1}{2}(\xi\tilde U-\tilde U_\xi)_\xi+\tilde U\tilde U_\xi=\tilde\chi(\tau)*\tilde P, \tag{23}$$

$$\tilde P_\tau+\tfrac{1}{2}(\xi\tilde P+\tilde P_\xi)_\xi+\tilde U\tilde P_\xi=\mathcal{F}\delta(\tau)\,\delta'(\xi)/\sqrt{T_0}, \tag{24}$$

where $\tilde\chi(\xi,\tau)=(T_0-T)^{3/2}\chi(x)$. The boundary conditions for $\tilde U$, $\tilde P$ are analogous to Eq. (8).

Let us describe now the general structure of the numerical scheme that finds the solution of our boundary problem. The diffusion terms $\tilde U_{\xi\xi}$, $\tilde P_{\xi\xi}$ in instanton equations (23),(24) have opposite signs. If one considers these equations as two linked Cauchy problems, then the natural direction of time in Eq. (23) is positive, while in Eq. (24) the direction is negative. Assume that at a given value of $\mathcal{F}$ the approximate solution $\tilde U_{\rm old}(\xi,\tau)$ is known. Let us try to make it closer to the true solution of the problem. For this purpose let us solve the Cauchy problem for Eq. (24) starting from $\tau=+0$ and moving up to large enough $\tau_{\min}<0$. Then using $\tilde P$ that we have got in the previous step we solve the Cauchy problem for Eq. (23) moving from $\tau=\tau_{\min}$ up to $\tau=0$. As a result we get the new values $\tilde U_{\rm new}(\xi,\tau)$. Further we will use the sign f for the mapping $\tilde U_{\rm old}\to\tilde U_{\rm new}$. The stationary point $\tilde U$ of the mapping f and the corresponding function $\tilde P$ are the desired solution of Eqs. (23),(24).

The numerical experiments have shown that iterations

$$\tilde U^{(i+1)}=f[\tilde U^{(i)}],\quad \tilde U^{(0)}\equiv 0 \tag{25}$$

converge if $\mathcal{F}>\mathcal{F}_*\simeq-0.96$. While $\mathcal{F}<\mathcal{F}_*$ the simple iterations (25) are divergent.

Curve 1 at the Fig. 1(a) shows how the value of the gradient $\tilde A=\partial\tilde U(\xi,\tau)/\partial\xi|_{\xi=0,\tau=0}$ depends on the number of iteration for $\mathcal{F}=-2$. It can be seen that the stationary point of f is unstable, but the mapping $f[f[\tilde U]]$ has two stable stationary points. The stability properties of the iterations are determined by the spectrum of the linearization $\hat K$ of f near a stationary point

$$f[\tilde U+V]=\tilde U+\hat K V+\cdots. \tag{26}$$

The iteration process is convergent if the modulus of all eigenvalues of the linear part $\hat K$ is less than 1. The period doubling indicates that while $\mathcal{F}$ passes through $\mathcal{F}_*$ one of $\hat K$'s eigenvalues passes through -1 [17]. Let us denote this eigenvalue as λ.

This knowledge allows us to construct the new mapping with stable stationary point that coincides with one of the mapping f. Let us proceed the following iterations:

$$\tilde U^{(i+1)}=f_c[\tilde U^{(i)}]\equiv cf[\tilde U^{(i)}]+(1-c)\tilde U^{(i)}, \tag{27}$$

where c is some constant. It is easy to check that the stationary points of the mappings f and f_c do coincide. The linear part of f_c is equal to $\hat K_c=c\hat K+(1-c)\hat 1$, its eigenvalue corresponding to unstable λ is $\lambda_c=c\lambda+(1-c)$. If we take the value of c inside the interval $0<c<2/(1-\lambda)<1$, then $|\lambda_c|<1$, and the iterations (27) are convergent.

Since we do not know λ *a priori*, the value of c that provides the convergence of iterations, was determined from experiment. Figure 1(a) illustrates the influence of the decreasing of c on the dependence of $\tilde A$ vs number of iteration. In the final version of the computer code the value of c was changed in an adaptive way: each time the value of $|\tilde A|$ was decreased after an iteration, c was multiplied by 0.9. One can compare from the Fig. 1(b) the iterations run for $c=0.1$, $c=0.05$ and for adaptive decreasing of c, all three for $\mathcal{F}=-2$. The initial and final values of c in the case of adaptive change were equal to 0.1 and $0.1\times0.9^4=0.05905\cdots$,

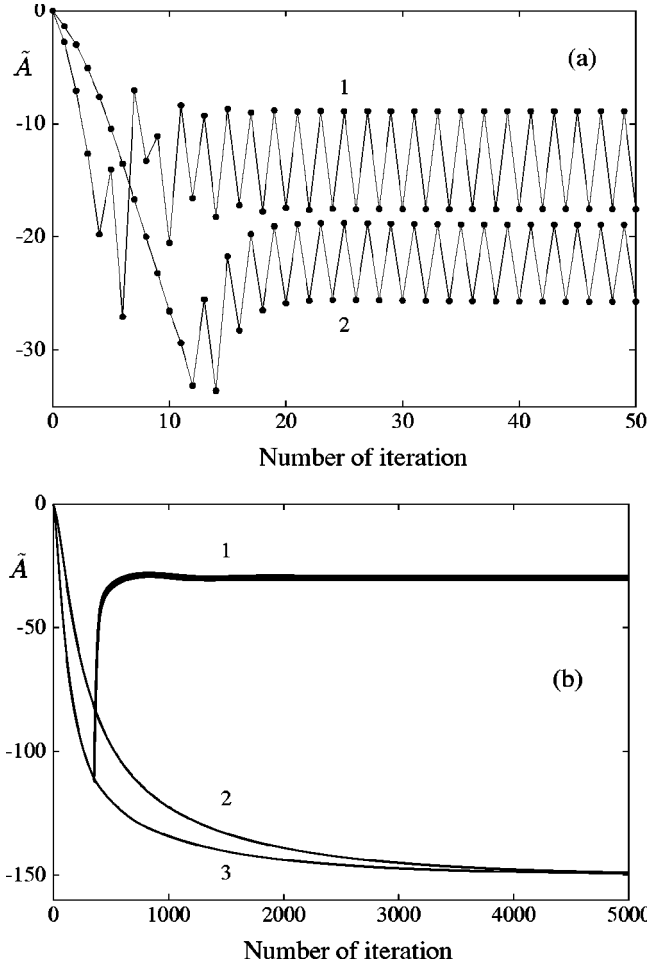

FIG. 1. The gradient $\tilde{A}$ as a function of number of iteration. (a) The dots corresponding to one run are joined by a line for convenience. The curves are: (a) simple iterations according to Eq. (25) (curve 1) and according to Eq. (27) with $c=0.1$ (curve 2); (b) $c=0.1$ (curve 1, its thickness is determined by the amplitude of serrated oscillations), $c=0.05$ (curve 2), and adaptive decreasing of c during the run, the initial value is $c=0.1$, c was multiplied by 0.9 four times (curve 3); $\mathcal{F}=-2$.

respectively. It is clear that for the two last cases the iterations converge to the same solution.

A. Grid parameters

The solution of Cauchy problem is found numerically using the method of finite differencies. The grid covers the rectangular domain $0<\xi<\xi_{\max}$, $\tau_{\min}<\tau<0$. In numerical calculations some of the boundary conditions (8) that in principle are posed at the infinity were considered as they are posed at (large enough) $\xi_{\max}$ and $\tau_{\min}$. Typical values used: $\xi_{\max}=10$ and $\tau_{\min}=-30$. The grid had uniform mesh intervals in ξ, typical number of grid sites along ξ axe was equal to 1024.

The first calculations had shown that the solution changes rapidly in the vicinity of $\tau=0$, while at large τ it varies slowly. Because of this we used nonuniform grid for variable τ. The time step was smaller inside the interval $\tau_1<\tau<0$, typical value used: $\tau_1=-0.4$. The number of grid sites inside this interval varied from 2000 to 4000. The computer power we had limited the number of all time steps in the grid by 5000. During all calculations we used $T_0=1$.

B. Cauchy problem for $\tilde{P}$

Equation (24) should be solved backward in time. The source term in the right-hand side of Eq. (24) provides us the initial condition $\tilde{P}(\tau=-0)\propto\delta'(\xi)$. This means that at small times the field $\tilde{P}$ is localized in a very narrow interval centered at $\xi=0$. Such initial condition can not be accurately discretized, so we used another way to represent $\tilde{P}$ at small times.

For small τ the field $\tilde{P}$ is very narrow. At its support we can approximate the velocity $\tilde{U}$ by a linear profile $\tilde{U}=\tilde{A}(\tau)\xi$. The evolution of $\tilde{P}$ in such a velocity field is described by the derivative of Gaussian contour

$$\tilde{P}(\xi,\tau)=\mathcal{F}\frac{\xi P_{\text{amp}}(\tau)}{\sqrt{2\pi T_0 D^3(\tau)}}\exp\left(-\frac{\xi^2}{2D(\tau)}\right), \tag{28}$$

$$P_{\text{amp}}(-0)=1, \quad D(-0)=0,$$

$$D(\tau)=\int_{\tau}^{0}d\tau'\exp\left(\int_{\tau'}^{\tau}d\tau''[2\tilde{A}(\tau'')+1]\right), \tag{29}$$

$$P_{\text{amp}}(\tau)=\exp\left(-\int_{\tau}^{0}d\tau'[2\tilde{A}(\tau')+1/2]\right). \tag{30}$$

We use such a representation for $\tilde{P}$ for $\tau_0<\tau<0$. The value of τ_0 is chosen in such a way, that the velocity field $\tilde{U}$ is still linear at the width of $\tilde{P}$. From the other hand, $\tilde{P}$ at $\tau=\tau_0$ already becomes wide in comparison with mesh interval $\Delta\xi$. Typical value of τ_0 used: $\tau_0=-1/1500$. For times $\tau<\tau_0$ the solution is found by fully implicit scheme

$$\frac{\tilde{P}_i^{n+1}-\tilde{P}_i^n}{\Delta\tau}+\frac{1}{2}\tilde{P}_i^{n+1}+D_i^{n+1}\frac{\tilde{P}_{i+1}^{n+1}-2\tilde{P}_i^{n+1}+\tilde{P}_{i-1}^{n+1}}{\Delta\xi^2}$$
$$+r_{+,i}^{n+1}\frac{\tilde{P}_{i+1}^{n+1}-\tilde{P}_i^{n+1}}{\Delta\xi}+r_{-,i}^{n+1}\frac{\tilde{P}_i^{n+1}-\tilde{P}_{i-1}^{n+1}}{\Delta\xi}=0, \tag{31}$$

where $r_{\pm,i}^n$, D_i^n are equal to

$$r_{\pm,i}^n=0.5[r(\xi_i,\tau_n)\pm|r(\xi_i,\tau_n)|],$$
$$D_i^n=\frac{1}{1+0.5|r(\xi_i,\tau_n)|\Delta\xi}. \tag{32}$$

The function $r(\xi,\tau)$ is expressed via velocity field $r(\xi,\tau)=0.5\xi+\tilde{U}(\xi,\tau)$.

Here $\Delta\xi>0$, $\Delta\tau<0$ are mesh intervals and ξ_i, τ_n are site coordinates. The numerical scheme used is monotonous and stable, it is of the first order of accuracy in $\Delta\tau$ and of the second order in $\Delta\xi$ [18].

C. Cauchy problem for $\tilde{U}$

At this stage we use the initial condition $\tilde{U}(\tau=\tau_{\min})\equiv 0$. The viscousity, source and self-advection terms are treated by splitting technique [19]. At each time step the change of $\tilde{U}$ due to the source is first calculated, then to the viscousity, and last to the nonlinearity.

From calculated already grid layer $\tilde{U}^n=\tilde{U}(\tau=\tau_n)$ the next layer $\tilde{U}^{n+1}$ is found in the following order. First, the equation $\tilde{U}_\tau=\tilde{\chi}(\tau)*\tilde{P}$, is solved:

$$\frac{\tilde{U}_i^{n+1}-\tilde{U}_i^n}{\Delta\tau}=[\tilde{\chi}(\tau)*\tilde{P}]_n. \tag{33}$$

The convolution $\tilde{\chi}*\tilde{P}$ is calculated as the result of inverse fast Fourier transform (FFT) acting on the product of $\tilde{\chi}$'s and $\tilde{P}$'s FFT images. The external force correlator during all calculations was equal to $\chi(x)=(1-x^2)e^{-x^2/2}=-d^2e^{-x^2/2}/dx^2$. The numbers $\tilde{U}_i^{n+1}$ that are found in such a way *are not* a final solution for the layer $\tilde{U}^{n+1}$, since only the source term has been taken into account yet. We use them as an input at the next step, we will denote them as $\tilde{U}_i^n$ [note that they *do not* coincide with $\tilde{U}_i^n$ in (33)].

Next, the viscousity and linear part of advection are taken into account, according to the equation $\tilde{U}_\tau+\frac{1}{2}(\xi\tilde{U}-\tilde{U})_\xi=0$. The fully implicit scheme was used analogously to Eq. (31):

$$\frac{\tilde{U}_i^{n+1}-\tilde{U}_i^n}{\Delta\tau}+\frac{1}{2}\tilde{U}_i^{n+1}-D_i\frac{\tilde{U}_{i+1}^{n+1}-2\tilde{U}_i^{n+1}+\tilde{U}_{i-1}^{n+1}}{\Delta\xi^2}+\frac{1}{2}\frac{\tilde{U}_i^{n+1}-\tilde{U}_{i-1}^{n+1}}{\Delta\xi}=0, \tag{34}$$

here $D_i=1/(1+0.25\xi_i\Delta\xi)$. Again, the numbers $\tilde{U}_i^{n+1}$ do not form a final solution, and we send them to the next step with a $\tilde{U}_i^n$ notation.

The nonlinear part of the equation $\tilde{U}_\tau+\tilde{U}\tilde{U}_\xi=0$ was solved by explicit conservative scheme [20]:

$$\frac{\tilde{U}_i^{n+1}-\tilde{U}_i^n}{\Delta\tau}+\frac{\tilde{U}_{i+1}^n+\tilde{U}_i^n+\tilde{U}_{i-1}^n}{3}\frac{\tilde{U}_{i+1}^n-\tilde{U}_{i-1}^n}{2\Delta\xi}=0, \tag{35}$$

that finally gives us the next layer of the velocity field $\tilde{U}^{n+1}$. This scheme is of the first order of accuracy in $\Delta\tau$ and of the second one in $\Delta\xi$.

IV. VISCOUS INSTANTON

In this section we represent the results of our calculations, that show the structure of the instanton and its change with $|\mathcal{F}|$. The minimal value of $\mathcal{F}$ at which the reliable results in numerics were obtained is $\mathcal{F}=-2$.

The general features of the instanton structure change with $\mathcal{F}$ can be obtained from Fig. 2 that shows the level curves of $\tilde{U}(\xi,\tau)$ for three values of $\mathcal{F}$. Since $\tilde{U}$ and $\tilde{P}$ are the odd functions of ξ, we draw only the region where $\xi>0$. The calculations were done in a rectangular $0<\xi<10$, $-30<\tau<0$, whose dimensions are a bit larger than it is shown at the figure.

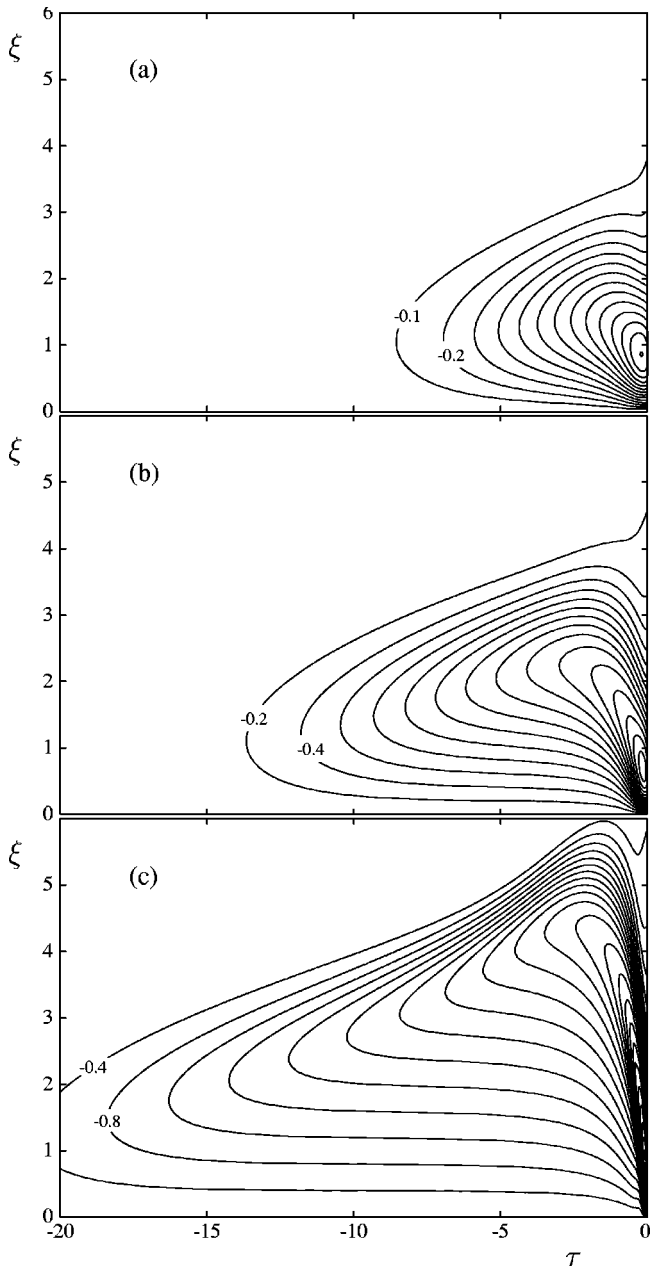

FIG. 2. The level curves if $\tilde{U}(\xi,\tau)$ for $\mathcal{F}=-0.9$ (a), $\mathcal{F}=-1.1$ (b), and $\mathcal{F}=-2$ (c). The values of levels can be calculated from the two given levels according to arithmetic progression law.

One can see that the instanton life-time and the maximal value of $|\tilde{U}|$ rapidly increase with the growth of $|\mathcal{F}|$. The growth leads to the deformation of level curves near $\tau=0$ because of the influence of nonlinearity, that is weak at $\mathcal{F}=-0.9$ [Fig. 2(a)] and very strong at $\mathcal{F}=-2.0$ [Fig. 2(c)].

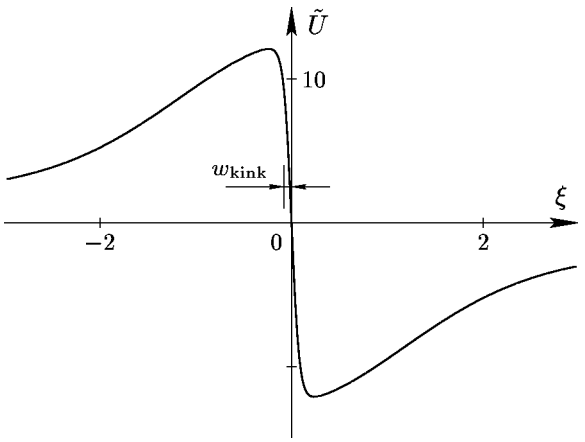

FIG. 3. The kink in the velocity field $\tilde{U}(\xi,\tau)$ at $\tau=0$; $\mathcal{F}=-2$.

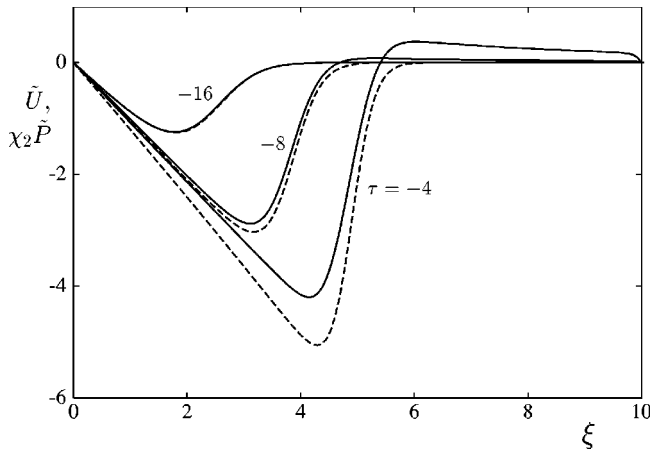

FIG. 4. Comparison of $\tilde{U}(\xi,\tau)$ (solid curves) and $\chi_2\tilde{P}(\xi,\tau)$ for three values of τ; $\mathcal{F}=-2$.

A. Structure

A detailed analysis of the instanton solution based on the results of numerical calculations allows us to distinguish five different regimes in the instanton time evolution. Below we discuss them consequently from $t=0$ to $t=-\infty$.

The first regime consist in the viscous smearing of the field p up to the scale of the kink width $w_{\text{kink}}=\sqrt{2\nu/|a|}=1/\sqrt{|A|}$ [see Eq. (12), Fig. 3]. Since the viscousity plays the crucial role in this regime, we will also use dimensional variables. At $t=-0$ we have $p(x,t)\propto\delta'(x)$, and the width of the kink in the velocity profile is equal to $w_{\text{kink}}=\sqrt{2\nu/|a|}$ [see Eq. (12)]. Since p is very narrow, the viscousity dominates the evolution. The width of p obeys the diffusion law and equals to $\sqrt{2\nu|t|}$. These two widths become comparable at time $t=-1/|a|$, or $T=-1/|A|$. This means that during the whole time of smearing of p by viscousity the width of the kink is of the order of w_{kink}. Indeed, if the shape of the velocity profile deviates from steady-state kink solution (12), then the change of the kink width during this time period would be of the order of $ut\sim\sqrt{2\nu|a|}/|a|=\sqrt{2\nu/|a|}=w_{\text{kink}}$. At this regime the source term χ^*P in instanton equation (10) is unimportant. When the width of p becomes of the order of w_{kink} the rate of expansion of p due to the velocity gradient becomes comparable with the rate due to viscousity (such a balance determines the width of the kink).

The next (second) regime was exhaustively studied in Ref. [4]. It consists in dilation of fields U, P up to the pump scale $L=1$. The fields are advected by velocity U, and considering evolution back in time they are expanded by it since $U_x|_{x=0}<0$. The time needed for the expansion is equal to $T_*\sim L/U\sim 1/\sqrt{|A|}$.

During the third through fifth regimes the width of U and P field is much greater than $L=1$. Then it is naturally to substitute $\chi(x)$ by $-\chi_2\delta''(x)$. The instanton equations take the following simple form:

$$U_T+UU_x+\tfrac{1}{2}V_{xx}=0,\quad V_T+UV_x+\tfrac{1}{2}U_{xx}=0,\qquad (36)$$

where $V=2\chi_2P-U$, $\chi_2=-\frac{1}{2}\int dx\,x^2\chi(x)$. While moving to large negative time numerical solution has a tendency to fall in $U=V$ (see Fig. 4, curves $\tau=-4$ and $\tau=-8$). Then the equations for U, V reduce to the Burgers equations with the evolution back in time.

Such a substitution is not always possible. During such an evolution the shock waves occur [see, e.g., the level curves at Fig. 2(c) near $\tau=-5$, Fig. 4, curves 1 and 2]. For transition to Eqs. (36) to be valid the width of these shock waves should be larger than $L=1$. Otherwise the substitution of χ by δ'' is not valid. The width of the shock wave in dimensionless variables is greater than 1 only if its height is smaller than 1. However, right after the second regime when the width of U and P fields becomes greater than the pumping force correlation length $L=1$ the amplitude of the velocity field U is of the order of $\sqrt{|A|}\gg 1$. The amplitude of U becames small only at very large times (it is shown below that such a crossover happens at $T\sim-\sqrt{|A|}$). It means that there is an intermediate regime that goes after the second one, where the substitution of χ by δ'' is inapplicable. In this (third) regime the fields U and P are smooth functions in the interval wider than 1. At the ends of this interval they contain shock waves—the value of U and P rapidly goes to zero (as it is shown schematically in Fig. 5). We will use the word "shock" for these structures at the ends of the interval, while for narrow structure in the velocity field U near $x=0$, $T=0$ we will use the word "kink."

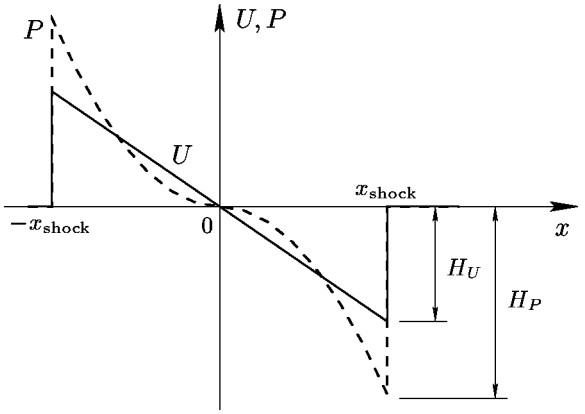

FIG. 5. Schematic representation of U and P for the third regime, $\mathcal{F}\to-\infty$.

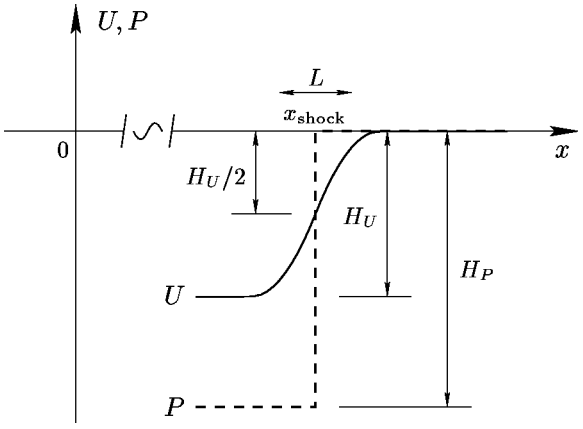

FIG. 6. Shock structure in the third regime, $\mathcal{F}\to-\infty$.

Now we will consider the structure of the shocks in detail. Let us denote the height of the shocks in $U(x,T)$ and $P(x,T)$ fields by $H_U(T)$ and $H_P(T)$, respectively. Their position we will denote as $x_{\rm shock}(T)$ ($x_{\rm shock}>0$, shocks are posed at $x=\pm x_{\rm shock}$).

In the third regime the width of the shocks in the field P is determined by the competition of squeezing them by the velocity U and spreading by viscousity (see Fig. 6). Since we are in a strongly nonlinear regime the viscousity is weak, and the width of P's shocks is very small. The shocks in P are stationed at the center of U's shocks, i.e., in almost linear velocity profile with the gradient $U_x\sim H_U$. The width of P's shocks can be estimated as $1/\sqrt{H_U}\ll L$. Then the good approximation for $P(x,T)$ near the shock $x\simeq x_{\rm shock}$ is $P(x,T)\simeq -H_P(T)\,\theta[x_{\rm shock}(T)-x]$, where $\theta(x)$ is the step function. During the evolution forward in time the shocks in U do not break down because of source term χ^*P. The source prevents the destructive effect of advection term UU_x. The shocks in P should carry the U's shocks of the height H_U, i.e., of strength $UU_x\sim H_U^2$. Thus we should have $H_P\propto H_U^2$ in this regime. Now we show it more carefully.

Let us write the instanton equation (10) in the reference frame of the shock near the point $x=x_{\rm shock}$ (see Fig. 6). We have two contributions to time derivative U_T: from the growth of H_U in time (of order H_U/T) and from the motion of the shock (of order H_U^2). Neglecting the first one we write the following equation for the velocity $U(x,T)$:

$$\frac{1}{2}[U(x)-U(x_{\rm shock})]_x^2=-H_P X'(x-x_{\rm shock}), \qquad (37)$$

where the new function $X(x)$ is determined by the equation $\chi(x)=-X''(x)$ with the condition $X\to 0$ with $x\to\pm\infty$. Integrating this equation once we obtain

$$[U(x)-U(x_{\rm shock})]^2=2H_P[X(0)-X(x-x_{\rm shock})]. \qquad (38)$$

Since $U(x_{\rm shock})=-H_U/2$ we have $H_P=H_U^2/8X(0)$.

The next step consists in finding the solution of Eqs. (10),(11) between the shocks posed at $x=\pm x_{\rm shock}$ considering the fields U, P as smooth ones and using the boundary condition

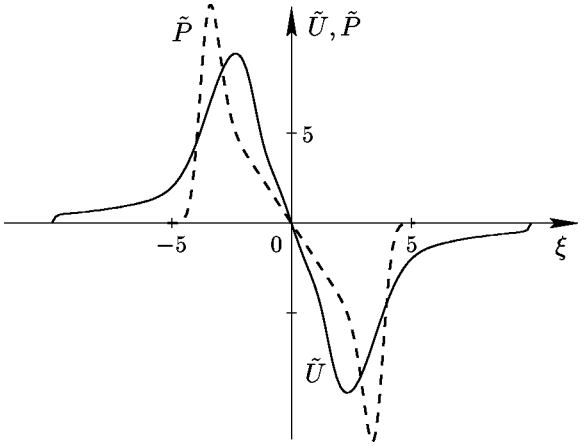

FIG. 7. $\tilde U(\xi)$ (solid curve) and $\chi_2\tilde P(\xi)$ (dashed curve) profiles at $\tau=-0.4$. $\mathcal{F}=-2$.

$$P(\pm x_{\rm shock}\mp 0,T)=\mp U^2(x_{\rm shock}-0,T)/8X(0). \qquad (39)$$

The instanton equations (10),(11) take the form

$$U_T+UU_x=0, \quad P_T+UP_x=0. \qquad (40)$$

Here we approximate the shocks as jump discontinuities, and the condition (39) relates the heights of the jumps (see Fig. 5). Here the diffusion terms and the term χ^*P are omitted. One can check that they are negligible since the characteristic x scale of the solution is large enough.

Equations (40) can be integrated by characteristics (or Lagrangian trajectories). The velocity of the shocks is equal to $\pm H_U/2$, i.e., all the trajectories disappear at the shocks (if we consider the evolution back in time). The value of U (or P) is conserved in time if we follow the Lagrangian trajectory. This means that the relation $P=U|U|/8X(0)$ holds everywhere between the shocks.

Due to self-advection the velocity field U became more and more linear as a function of x while $|T|$ increases. This happens at the border between the second and the third regimes. In the third regime we can take $U(x,T)=x/T$ between the shocks. The field P is equal to $P(x,T)=-x|x|/8X(0)T^2$. The velocity U simply squeezes or expands the field P without changing its shape. Since $H_P\sim H_U^2$, the field P should have the same scaling as U^2, i.e., $P\propto x^2$. The concave form of P (as one can see $\mathcal{F}=-2$ is not yet good enough for a clear picture) is shown in Fig. 7.

Let us determine the time dependence of $x_{\rm shock}$. We have

$$\frac{dx_{\rm shock}}{dT}=-\frac{1}{2}H_U(T)=-\frac{x_{\rm shock}}{2T}. \qquad (41)$$

Solving this equation we get $x_{\rm shock}(T)=B\sqrt{-T}$. Since $x_{\rm shock}\sim 1$ at $|T|\sim 1/\sqrt{|A|}$, we get $B\sim|A|^{1/4}$. The shocks heights are equal to $H_U(T)=B/\sqrt{-T}$, $H_P(T)=B^2/8X(0)|T|$. The width of the shocks in P field is of the order of $1/\sqrt{H_U}$. The shocks in velocity field U have the width of the order of 1, since U is pumped by χ^*P.

At large time $T\sim-\sqrt{|A|}$ the height H_U (and consequently the width of the shocks in P) became of the order of 1. This

indicates the end of the third regime and the beginning of the fourth. Going further back in time we finally enter the domain of validity of Eq. (36). The solution falls into $U=V$. Again, the solution has two shocks between which it is a smooth function. The shock position satisfies $x_{\text{shock}} \propto \sqrt{-T}$, between the shocks $U=V=x/T$ holds. This regime exactly corresponds to self-similar solution $u(x,t)=\theta(t-Cx^2)x/t$ of inviscid Burgers equation $u_t+uu_x-0\cdot u_{xx}=0$ (here C is a parameter).

At the far tail of the instanton due to viscous dissipation the solution $U=V$ transforms to the derivative of Gaussian contour — the self-similar solution of the diffusion equation (see Fig. 4, $\tau=-16$). During the fifth regime the advection term UU_x becomes irrelevant. In ξ, τ variables the solution tends to $\tilde{U} \propto \xi \exp(\pi/2-\xi^2/2)$, that was observed in numerical calculations.

During the fourth and the fifth regimes the amplitude of the velocity field U is less than unity. It means that the amplitude of U is lower than the order of the typical statistical fluctuations, and the saddle-point approximation is meaningless there. The typical events that demonstrate large negative gradients start from some velocity configuration $U(x)$ with the amplitude of the order of unity and are governed by the third regime first. The action on these events and their further evolution almost do not depend on the initial velocity field $U(x)$, and the dependence of $\mathcal{P}(a)$ on a remains unaltered by the averaging over all possible configurations $U(x)$. We considered the 4th and the 5th regimes since they are the parts of the whole solution of our nonlinear boundary problem.

Let us now run the whole evolution forward in time. At the beginning (fifth regime) the field U is pumped by very wide P. The pumping force is proportional to P_{xx}. During the fourth regime the source is localized at shocks in P that leads to a formation of shocks in U. The U's shocks want to break down because of self-advection, but the source term $\chi^* P$ keeps them going. When the growing height of P becomes larger than unity the shocks in P become narrow. The balance between the terms UU_x and $\chi^* P$ in Eq. (10) changes a little, that results in the change of the form of U's shocks — it is determined by the shape of $\chi(x)$ now. The distance between the P's shocks decreases in time and eventually it becomes comparable with unity. After this P becomes even more narrow and the efficiency of the source term begins to fall down. The self-advection of the velocity destroyes the shocks and leads to a formation of the kink at $x=0$, while P transformes to $\delta'(x)$. The kink shape at $\mathcal{F}=-2$ is shown in Fig. 3. Schematically time evolution of the instanton is illustrated in Fig. 8.

B. Action

One can present the action $S(A)$ in the form of $S=\int_{-\infty}^{0} dT\, s(T)$ as in expression (14). For $\mathcal{F}=-2$ the action density $s(T)$ that was obtained from numerical calculations is shown in Fig. 9. While $T<T_*=-1/\sqrt{|A|}$ the convolution $\chi^* p$ is localized at shocks, so $s(T) \sim H_P^2(T) \sim B^4/T^2$. The maximum of $s(T)$ is posed at $T \sim T_*$. Further increasing T leads to the decreasing of the density $s(T)$ because $P(x)$

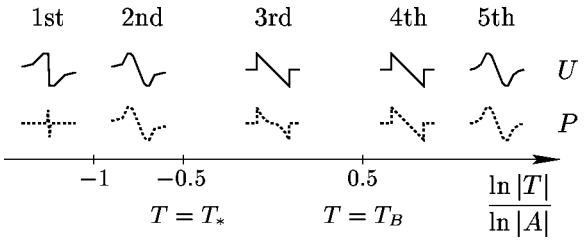

FIG. 8. Schematic representation of the instanton time structure.

becomes more and more narrow without an adequate growth of its amplitude. This region of small time $T>T_*$ was studied in Ref. [4]. It was shown that the contribution $S_{T>T_*}$ to the extremal action from this interval is of order $|A|^{3/2}$, and the main contribution to the action from it comes from the region $T \sim T_*$ — the border between the second and the third regimes. Exactly these two regimes determine the optimal configuration of noise providing the event with large negative gradient.

The contribution of region of time $-\sqrt{|A|}=T_B<T<T_*=-1/\sqrt{|A|}$ (third regime) to the extremal action $S(A)$ can be estimated as

$$S_{T<T_*} \sim \int_{T_B}^{T_*} dT\, H_P^2(T) \sim -B^4/T_* \sim |A|^{3/2}. \qquad (42)$$

Note that the value of $S_{T<T_*}$ is again cumulated from the region $T \sim T_*$. The crucial point is that the contribution to the action $S(A)$ from the tail of the instanton (or large time $T<T_*$) is finite, i.e., the integral (42) converges (the addition to the action from interval $T<T_B$ is negligible). Also this contribution is not dominant, i.e., it is not much greater than the contribution of the order $|A|^{3/2}$ from small times ($T>T_*$). It means that in our case the instanton is localized enough in time. Its long-time dynamics does not destroy the fact that it is the main fluctuation determining the statistics of large negative gradients.

At the Fig. 10 the function $d(\ln S)/d(\ln A)=\mathcal{F}A/S$ that was obtained from numerical calculations is shown. We used different grid parameters during calculations for instanton struc-

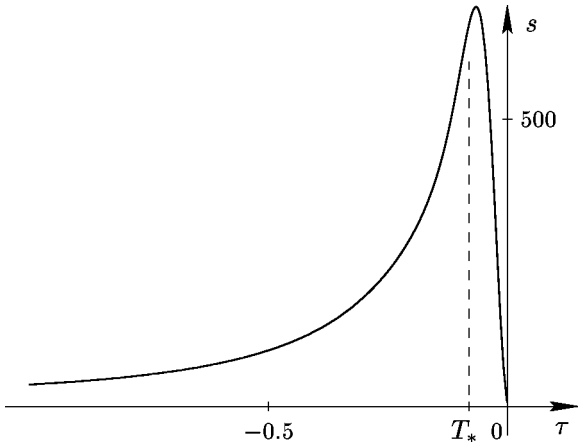

FIG. 9. The action density $s(\tau)$ as a function of "time" τ. $\mathcal{F}=-2$.

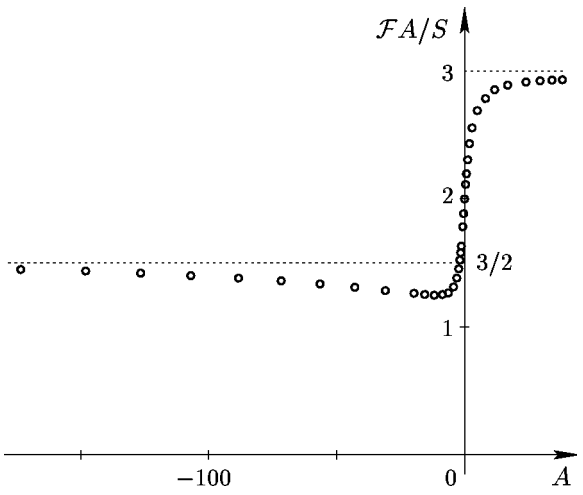

FIG. 10. $\mathcal{F}A/S = d(\ln S)/d(\ln A)$ [see Eq. (16)] as a function of gradient A.

ture and for this figure. Here we used $\tau_{\min} = -4$ with boundary condition $\tilde{U}(\xi, \tau_{\min}) = \chi_2 \tilde{P}(\xi, \tau_{\min})$. This boundary condition was used as initial condition for $\tilde{U}$ during iterations. It turned out, that e.g. for $\mathcal{F} = -2$ we get the following values of $\mathcal{F}A/S$ and A with different value of $\tau_{\min}$:

$\tau_{\min}$	$\mathcal{F}A/S$	A
-4	1.441	-148.1
-30	1.437	-102.6

Although, when calculating with $\tau_{\min} = -30$, the condition $\tilde{U}(\xi, -4) = \chi_2 \tilde{P}(\xi, -4)$ holds within 15% (as one can see from Fig. 4) we prefer to use the grid shorter in time ($\tau_{\min} = -4$) to have smaller time step. The value of A strongly depends on time step. It was observed in numerical experiment. Such sensitivity is characteristic of Burgers equation also. Although the calculations with small $|\tau_{\min}|$ give us worse accuracy at the tail of the instanton, the smallness of the time step allows us accurately describe the main part of the instanton where the nonlinearity level is high.

One can see the cubic asymptotics $S \propto A^3$ at $A > 0$. The instanton structure for $A > 0$ that was described in Refs. [3,4] was confirmed by our numerical calculations. The case $A < 0$ corresponding to the PDF's left tail is more complicated. The function $\mathcal{F}A/S$ has minimal value at $A \simeq -12$. At further decrease of A it starts to grow and finally tends to the value 3/2. In this case the coefficient $S/|A|^{3/2}$ is small.

V. CONCLUSION

We have examined the remote left tail of the velocity gradients PDF $\mathcal{P}(u_x)$ in Burgers forced turbulence. The possibility of direct numerical solving of instanton equations by iterations is demonstrated. Numerical calculations and the analysis of the instanton behavior at the time large compared with its lifetime $t_* \sim 1/\sqrt{\nu |u_x|}$ with the solution at small time from Ref. [4] show that $\ln \mathcal{P}(u_x) \propto -|u_x|^{3/2}$.

ACKNOWLEDGMENTS

We are grateful to G.E. Falkovich, A.V. Fouxon, I.V. Kolokolov, V.V. Lebedev, and E.V. Podivilov for useful discussions. This work was partially supported by Russian Foundation for Basic Research (Grant No. 98-02-17814), by INTAS (M.S., Grant No. 96-0457) within the program of International Center for Fundamental Physics in Moscow, by the grants of Minerva Foundation, Germany and Mitchell Research Fund (M.S.).

[1] J.M. Burgers, *The Nonlinear Diffusion Equation* (Reidel, Dordrecht, 1974).
[2] A.M. Polyakov, Phys. Rev. E **52**, 6183 (1995).
[3] V. Gurarie and A. Migdal, Phys. Rev. E **54**, 4908 (1996).
[4] E. Balkovsky, G. Falkovich, I. Kolokolov, and V. Lebedev, Phys. Rev. Lett. **78**, 1452 (1997).
[5] S.A. Boldyrev, Phys. Rev. E **55**, 6907 (1997).
[6] W. E, K. Khanin, A. Mazel, and Ya. Sinai, Phys. Rev. Lett. **78**, 1904 (1997).
[7] T. Gotoh and R.H. Kraichnan, Phys. Fluids **10**, 2859 (1998).
[8] M.V. Feigel'man, Zh. Éksp. Teor. Fiz. **79**, 1095 (1980) [Sov. Phys. JETP **52**, 555 (1980)].
[9] R. Kraichnan, Phys. Fluids **11**, 3738 (1999); W. E and E. Vanden Eijnden, *ibid.* **12**, 149 (2000).
[10] I.M. Lifshitz, Usp. Fiz. Nauk **83**, 617 (1964) [Sov. Phys. Usp. **7**, 549 (1965)].
[11] L.N. Lipatov, Zh. Éksp. Teor. Fiz. **72**, 411 (1977) [Sov. Phys. JETP **45**, 216 (1977)].
[12] G. Falkovich, I. Kolokolov, V. Lebedev, and A. Migdal, Phys. Rev. E **54**, 4896 (1996).
[13] M. Chertkov, Phys. Rev. E **55**, 2722 (1997); E. Balkovsky and V. Lebedev, *ibid.* **58**, 5776 (1998).
[14] I.V. Kolokolov, Pis'ma v Zh. Éksp. Teor. Fiz. **71**, 20 (2000) [JETP Lett. **71**, 12 (2000)].
[15] P.C. Martin, E.D. Siggia, and H.A. Rose, Phys. Rev. A **8**, 423 (1973); C. de Dominicis, J. Phys. (Paris), Colloq. **37**, C-1, 247 (1976); H. Janssen, Z. Phys. B: Condens. Matter **23**, 377 (1976); C. de Dominicis and L. Peliti, Phys. Rev. B **18**, 353 (1978).
[16] L.V. Keldysh, Zh. Éksp. Teor. Fiz. **47**, 1515 (1964) [Sov. Phys. JETP **20**, 1018 (1965)].
[17] V.I. Arnold, *Geometrical Methods in the Theory of Ordinary Differential Equations* (Springer, New York, 1988).
[18] A.A. Samarskii and A.V. Gulin, *Numerical Methods* (Nauka, Moscow, 1989).
[19] R. Temam, *Navier-Stokes Equations. Theory and Numerical Analysis* (North-Holland, Amsterdam, 1979).
[20] C.A.J. Fletcher, *Computational Galerkin Methods* (Springer-Verlag, New York, 1984).